Density functional theory based effective fragment potential method

Ivana Adamovic, Mark A. Freitag, and Mark S. Gordon

Citation: The Journal of Chemical Physics **118**, 6725 (2003); doi: 10.1063/1.1559912
View online: http://dx.doi.org/10.1063/1.1559912
View Table of Contents: http://scitation.aip.org/content/aip/journal/jcp/118/15?ver=pdfcov
Published by the AIP Publishing

Density functional theory based effective fragment potential method

Ivana Adamovic, Mark A. Freitag,[a] and Mark S. Gordon[b]
Department of Chemistry, Iowa State University, Ames, Iowa 50011

(Received 9 December 2002; accepted 21 January 2003)

The effective fragment potential (EFP) method, is a discrete method for the treatment of solvent effects, originally formulated using Hartree–Fock (HF) theory. Here, a density functional theory (DFT) based implementation of the EFP method is presented for water as a solvent. In developing the DFT based EFP method for water, all molecular properties (multipole moments, polarizability tensors, screening parameters, and fitting parameters for the exchange repulsion potential) are recalculated and optimized, using the B3LYP functional. Initial tests for water dimer, small water clusters, and the glycine–water system show good agreement with *ab initio* and DFT calculations. Several computed properties exhibit marked improvement relative to the Hartree–Fock based method, presumably because the DFT based method includes some dynamic electron correlation through the corresponding functional. © *2003 American Institute of Physics.*
[DOI: 10.1063/1.1559912]

I. INTRODUCTION

An increasingly important area in quantum chemistry applications is the development of methods that are capable of accurate treatment of solvent effects. There are two main approaches to solvation: continuum[1] and discrete methods.[2] Both of these have advantages and disadvantages. The continuum methods are fast, and they are designed to reproduce bulk properties of the solvent. On the other hand, continuum methods can be very sensitive to cavity parameters and they cannot describe the individual interactions between solute and solvent molecules. The discrete methods treat these interactions successfully, but they can be computationally demanding, if *ab initio* potentials are used, or require many empirical parameters, and they may require extensive configurational sampling.

The development of methods for modeling hydrogen-bonded systems plays a key role in studies of a vast range of chemical and biological processes in solution. Most of these processes take place in water, so understanding and being able to predict the properties of the water, as well as to treat reactions in aqueous solution is one of the crucial challenges in modern quantum chemistry. The effective fragment potential (EFP) method[3] is a discrete solvation approach that was designed to treat chemical reactions in solution.[3,4(a),4(b)] However, the EFP method has also been used to study solvent clusters,[5(a),5(b)] solvent effects on excited states of biomolecules,[6] neutral–zwitterion equilibrium in amino acids,[9(a),9(b)] treatment of the covalent bond in proteins,[7,8] and recently it was interfaced with a continuum method (PCM).[9] The original method (referred as EFP1/HF) was designed specifically for the solvent water at the Hartree–Fock (HF) level of theory. The problems to which the EFP1 method has been applied have revealed broad success in reproducing the corresponding HF results. However, the HF method itself is of limited use, because correlation effects are not included at this level of theory.

Therefore, the next logical step in the development of the EFP method would be inclusion of some correlation effects. A popular approach for including correlation effects via correlation functionals is density functional theory (DFT).[10] So, the new EFP formulation described here is based on DFT, using the B3LYP functional.[11,12] DFT/B3LYP has been shown to reproduce hydrogen bonding interactions with an acceptable accuracy.[10(b)] The advantage of a DFT based EFP method is that DFT includes some (short-range) correlation effects, while the cost of the calculation is comparable with that of HF calculations. The primary motivation for developing a DFT based EFP is a more accurate treatment of chemical processes in water, as well as improving the binding energies of water clusters.

A brief overview of the EFP1 method, together with a description of all relevant energy terms, is given in Sec. II. This section is followed by a presentation of the DFT based properties and parameters. Applications of the DFT based EFP method to the water dimer, small water clusters, and glycine are presented in the subsequent section of the paper.

II. OVERVIEW OF THE EFP METHOD

The original effective fragment potential (EFP1/HF) is represented by a set of one-electron potentials that are added to the *ab initio* electronic Hamiltonian. The EFP contains three energy terms: (1) Coulombic interactions between solvent molecules (fragment–fragment) and solvent molecules with quantum mechanical (QM) solute molecules (fragment–QM), including charge penetration, which corrects for the pointwise nature of the electrostatic expansion, (2) polarization or induction interaction between solvent molecules (fragment–fragment) and solvent molecules with QM solute molecules (fragment–QM), and (3) exchange re-

[a]Current address: Department of Chemistry, Creighton University, Omaha, Nebraska 68178.
[b]Author to whom correspondence should be addressed. Electronic mail: mark@si.fi.ameslab.gov

pulsion, charge transfer and other energy terms that are not taken into account in (1) and (2). The latter is referred to as the remainder term. The Coulomb, polarization and charge penetration (screening) contributions are determined entirely from *ab initio* calculations on the water monomer. The exchange–repulsion/charge transfer term is determined by a fitting procedure to the QM potential of the water dimer. A more general, EFP2 method avoids fitting procedure.[13–16]

A schematic of the EFP method is given as[3,4]

$$H_{\text{total}} = H_{\text{QM}} + V. \tag{1}$$

The system is divided into two parts: a QM region, H_{QM}, which could include some of the solvent molecules, and the rest of the solvent molecules represented as a fragment potential, V. In the QM part one can use any level of theory, but the most consistent approach is to use the same level of theory as the one from which the potential was derived (e.g., HF or DFT).

As noted above, the fragment potential consists of Coulomb, polarization, and remainder contributions, respectively, as shown in the following:

$$V_{\text{el}}(\mu,s) = \sum_{k=1}^{K} V_k^{\text{elec}}(\mu,s) + \sum_{l=1}^{L} V_l^{\text{pol}}(\mu,s) + \sum_{m=1}^{M} V_m^{\text{Re}\,p}(\mu,s), \tag{2}$$

where s is a coordinate of the QM part. For the μth solvent molecule, these contributions are expanded over a number (K, L, M) of expansion points. Each of these terms will be explained in detail in the next section. The analogous terms are derived for nuclei–fragment and fragment–fragment interactions.[13–16]

A. Electrostatic interactions

A distributed, multicenter, multipolar expansion[17] of the molecular density is used as a compact description of the Coulomb potential. The expansion is carried out through octopole moments at $K=5$ points for the water molecule (nuclear centers and bond midpoints). The expression for the electrostatic potential is as follows:

$$V_k^{\text{elec}}(\mu,s) = \frac{q_k(\mu) q_s}{r_{sk}} - \sum_{\alpha}^{x,y,z} \mu_\alpha^k(\mu) F_\alpha(r_{sk}) - \frac{1}{3} \sum_{\alpha,\beta}^{x,y,z} \Theta_{\alpha\beta}^k(\mu) \times F_{\alpha\beta}(r_{sk}) - \frac{1}{15} \sum_{\alpha,\beta,\gamma}^{x,y,z} \Omega_{\beta\gamma}^k(\mu) F_{\alpha\beta\gamma}(r_{sk}), \tag{3}$$

where q, μ, Θ, and Ω are the charge, dipole, quadrupole, and octopole moments for the fragment, respectively, and F_a, F_{ab}, and F_{abc} are the QM electric field, field gradient, and field Hessian.

For the DFT based EFP the multipole moments were calculated using the Kohn–Sham density. For example,

$$\mu_\alpha = \int \rho(r) r_\alpha \, d^3r, \tag{4}$$

$$\Theta_{zz} = \int \rho(r) r^2 \left(\frac{3}{2}\cos^2\theta - \frac{1}{2} \right) d^3r, \tag{5}$$

where μ_α is a component of the dipole moment, Θ_{zz} is a component of the quadrupole tensor,[17] and $\rho(r)$ is the Kohn–Sham density. Analogous expressions may be written for the higher moments.

B. Charge penetration

The distributed multipolar analysis (DMA) is a pointwise model. Therefore, it cannot account for the overlap of the charge densities between two molecules, as they approach each other. For long distances between molecules the DMA gives a good description of the electrostatic interaction, but it needs to be corrected at shorter distances, at which the actual charge densities would overlap. One way to correct this is to introduce a screening function. In EFP1/DFT the charge–charge interaction is screened. In this approach, the Coulomb term is multiplied by a damping function, which is chosen to have the following form:

$$V_k^{\text{elec}}(\mu,s) \rightarrow [1 - c_k(\mu) e^{-\alpha_k(\mu) r_{sk}^2}] V_k^{\text{elec}}(\mu,s), \tag{6}$$

where V_k^{elec} is that part of the Coulomb potential that contains only the charge–charge term.

In EFP1/HF the same function is used to calculate the QM–fragment and fragment–fragment charge penetration.[3] In EFP1/DFT the damping function in Eq. (6) is used for the QM–fragment term. For the fragment–fragment charge penetration a more general expression,[18] which can be applied to any solvent, is used. For the general case of two different fragments ($\alpha_A \neq \alpha_B$):

$$E_{\text{chg-chg}}^{\text{Pen}} = -\frac{1}{2R_{AB}} \Big[q_A(q_B + 2Z_B) e^{-\alpha_A R_{AB}} + q_B(q_A + 2Z_A) e^{-\alpha_B R_{AB}} + \frac{q_A q_B(\alpha_A^2 + \alpha_B^2)}{\alpha_A^2 - \alpha_B^2} (e^{-\alpha_B R_{AB}} - e^{-\alpha_A R_{AB}}) \Big]. \tag{7}$$

For the same fragments ($\alpha_A = \alpha_B$) the energy formula becomes

$$E_{\text{chg-chg}}^{\text{Pen}} = -\frac{1}{R_{AB}} \Big[q_A q_B \Big(1 + \frac{\alpha R_{AB}}{2} \Big) + q_A Z_B + q_B Z_A \Big] e^{-\alpha R_{AB}}. \tag{8}$$

C. Polarization/induction

The second EFP energy contribution is the polarization energy. Polarization, or induction, is treated by a self-consistent perturbation model, using localized molecular orbital (LMO) polarizabilities.[3] The molecular polarizability tensor is expressed as a tensor sum of the LMO polarizabilities, centered at the LMO centroids. For water, there are five such LMOs: oxygen inner shell, two oxygen lone pairs, and two oxygen–hydrogen bonds. Numerical, finite field calculations, using these LMOs, on an isolated water molecule, provide the total dipole polarizability tensor, using the equations

$$\mu = -2\sum_{l} [\langle \chi_l' | r | \chi_l' \rangle - \langle \chi_l^0 | r | \chi_l^0 \rangle], \tag{9}$$

$$\alpha_{xx'} = \lim_{F_x \to 0} \frac{\mu_x}{F_{x'}}, \tag{10}$$

$$\alpha_{xx'} = \sum_{l}^{\text{LMOs}} \alpha_{xx'}^{l}, \tag{11}$$

where χ and χ^0 are the perturbed and unperturbed LMOs, respectively, F is the applied electric field, μ is the dipole moment, and α is the linear polarizability. Once the polarizability components of the fragment molecule have been determined, the polarization energy is calculated to self-consistency:

$$V_l^{\text{Pol}}(\mu) = -\sum_{\alpha,\beta}^{x,y,z} F_\alpha(r_l)\alpha_{\alpha\beta}^{l}(\mu)\langle F_\beta(r_l)\rangle \tag{12}$$

Here, F_b is the field due to the QM part of the system, and α_{xy}^{l} is xy component of the dipole polarizability tensor of the fragment molecule in the lth localized orbital.

D. Exchange repulsion/charge transfer

The remaining term contains all interactions not accounted for by the Coulomb and polarization terms. For EFP1/HF these represent exchange repulsion and charge transfer. For EFP1/DFT there are also some short range correlation contributions to the remainder term. For the QM–fragment interaction this term $V_m^{\text{REP}}(\mu,s)$ is represented by a linear combination of two Gaussian functions, expanded at the atom centers,

$$V_m^{\text{rep}}(\mu,s) = \sum_{j}^{J} c_{m,j}(\mu) e^{-\alpha_{m,j}(\mu) r_{m,s}^2}, \tag{13}$$

where μ and s are fragment and QM (DFT) coordinates, respectively.

For the fragment–fragment interaction instead of two Gaussian functions, a single exponential is used and the expansion is done at the atom centers and the center of mass, in order to better capture the angular dependence of the charge transfer contribution. To optimize coefficients and exponents in these model potentials the DFT energy was first calculated for 192 points on the water dimer potential energy surface. These points were chosen so as to span several O–O distances for several H_2O–H_2O orientations. For the same set of points the Coulomb and polarization energy contributions were calculated for the DFT–fragment and fragment–fragment interactions. The repulsion potential, V_m^{REP}, Eq. (13), is then fitted to the difference between the total DFT energy and the sum of the Coulomb and polarization contributions:

$$\Delta = \sum_{p}^{P} w_p \left[\langle \Psi | \sum_{m}^{M} V_m^{\text{Re}\,p} | \Psi \rangle - E_{\text{rep}}^{(\text{QM})}(p) \right]^2, \tag{14}$$

where w_p is a weighting function and Ψ is the wave function for the QM (DFT) region. Details regarding this fitting process are given in Sec. III.

TABLE I. Monopole moments for the water effective fragment in a.u. The expansion points O (0.000 00, 0.000 00, −0.119 151), H (−1.431 042, 0.000 00, 0.945 51), H (1.431 042, 0.000 00, 0.945 51), BO21 (−0.715 521, 0.000 00, 0.413 179), and BO31 (0.715 521, 0.000 00, 0.413 179) are oxygen and hydrogen atoms and the bond midpoints, respectively, with the coordinates given in parentheses (bohr).

Monopoles	DFT	HF	MP2
O	−8.224 578	−8.210 826	−8.224 102
H	−0.579 055	−0.556 652	−0.577 175
H	−0.579 055	−0.556 652	−0.577 175
BO21	−0.308 655	−0.337 934	−0.310 772
BO31	−0.308 655	−0.337 934	−0.310 772

E. Computational details

In order to develop the EFP1/DFT method it was necessary to choose a functional, on which to base the model. Since the B3LYP functional is very popular, this functional was chosen with the Dunning–Hay (DH) basis set,[19] with *d* polarization functions on oxygen atom and *p* polarization on hydrogen atoms, to be consistent with the EFP1/HF method. The geometry of the fragment water molecule is fixed with bond lengths of 0.9468 and a bond angle of 106.70°.

The derivation and coding of the energy gradient for the general charge penetration of the fragment–fragment interaction were completed, so that geometry optimizations can be performed. All calculations were done using the electronic structure code GAMESS.[20]

III. RESULTS AND DISCUSSION

A. Electrostatic energy

As noted previously, five points (atom centers and bond midpoints) were used in the expansion of the Coulomb energy up to octopoles. Charges (monopole moments) obtained from DFT, HF and second order perturbation theory (MP2) are presented in Table I. A similar analysis was done for all multipoles, up to the octopole moments, and Table II compares the components of the dipole moment. The agreement for the higher moments is similar to that of the lower one. The most important observation is that the three methods are in reasonably good agreement, as was expected for the Coulomb interaction. The DFT results are on average between the HF and MP2 results.

B. Charge penetration

The general strategy for the optimization of the coefficients and exponents of the screening function is as follows: DFT and classical Coulomb potentials (using the distributed multipolar expansion) were generated on a number of grid points. The damped classical potential is then fitted so that the difference between it and the DFT potential is minimized according to

$$\Delta = \sum_{\text{grid point}} [V_{\text{QM}}^{\text{ES}} - V_{\text{damped DMA}}^{\text{ES}}]^2. \tag{15}$$

For the DFT–fragment interaction, the damping function has a Gaussian form, while for the fragment–fragment

TABLE II. Components of the dipole moment for the water effective fragment in a.u. First line is HF, second DFT, and third MP2 results.

	μ_x	μ_y	μ_z
O	0.000 000	0.000 00	0.439 368
	0.000 000	0.000 00	0.435 527
	0.000 000	0.000 00	0.439 230
H	−0.045 030	0.000 00	0.019 745
	−0.053 498	0.000 00	0.026 668
	−0.050 851	0.000 00	0.022 763
H	0.045 030	0.000 00	0.019 745
	0.053 498	0.000 00	0.026 668
	0.050 851	0.000 00	0.022 763
BO21	0.151 206	0.000 00	−0.116 204
	0.145 227	0.000 00	−0.106 533
	0.146 305	0.000 00	−0.110 169
BO21	−0.151 206	0.000 00	−0.116 204
	−0.145 227	0.000 00	−0.106 533
	−0.146 305	0.000 00	−0.110 169

interaction[18] the function is a simple exponential. The number of grid points in this optimizations is 15 724 and the grid spacing is chosen to be 0.50 Bohr. Grid points were distributed in the spherical shell between two spheres around each atom. The radii of the spheres are called $R_{\min}$ and $R_{\max}$. During the optimization procedure $R_{\min}$ and $R_{\max}$ were varied and the final values of these parameters were set to 67% of the van der Waals radius for $R_{\min}$ and 300% for $R_{\max}$. The fitting statistics are given in Table III. The RMS deviations are less than 1 kcal/mol. Optimized coefficients and exponents for the fragment–fragment potential are given in Table IV and for the DFT–fragment potential in Table V.

C. Charge penetration gradient for the fragment–fragment interaction

The energy gradient for the general case of different exponents ($\alpha_A \neq \alpha_B$) is given by

$$\frac{\partial E}{\partial X} = \frac{e^{-(\alpha_A+\alpha_B)R_{AB}}}{(\alpha_A^2-\alpha_B^2)R_{AB}^2} \times\{q_B e^{\alpha_A R}(1+\alpha_B R_{AB})[q_A\alpha_A^2+Z_A(\alpha_A^2-\alpha_B^2)] + q_A e^{\alpha_B R}(1+\alpha_A R_{AB})[Z_B(\alpha_A^2-\alpha_B^2)-q_B\alpha_B^2+]\}. \quad (16)$$

If the expansion points are the same ($\alpha_A=\alpha_B$) the above expression becomes

TABLE III. Fitting statistics for the charge penetration. Averaged error and RMS deviations of the fitting procedures in kcal/mol.

DFT–fragment statistics		Fragment–fragment statistics	
Averaged unsigned error	1.356 644$E-01$	Averaged unsigned error	1.777 169$E-01$
RMS deviation (all 15 724 points)	9.074 347$E-01$	RMS deviation (all 15 724 points)	9.979 120$E-01$

TABLE IV. Fragment–fragment screening parameters.

	Coefficient	α (exponent)
O	1.000 000	1.960 183
H	1.000 000	2.383 508
H	1.000 000	2.383 508
BO21	1.000 000	9.999 913
BO31	1.000 000	9.999 913

$$\frac{\partial E}{\partial X} = \frac{e^{-\alpha R_{AB}}}{R_{AB}^3} \times\left[(q_A q_B+q_A Z_B+q_B Z_A)(1+\alpha R_{AB})+\frac{q_A q_B R_{AB}^2\alpha^2}{2}\right], \quad (17)$$

where α_A and α_B are coefficients of the exponential function, q_A and q_B are fragment charges and Z_A and Z_B are nuclear charges.

D. Polarization

To model the induction interaction, the LMO polarizabilities were calculated at five expansion points: oxygen inner shell, two lone pairs on oxygen, and two oxygen–hydrogen bonds. The Boys[21] localization scheme was used to localize Kohn–Sham orbitals. A finite field, numerical procedure was applied to extract the LMO polarizabilities at the centroids of charge. The results for the LMO polarizability tensors are presented in Table VI.

E. Exchange–repulsion/charge transfer (remainder term)

The remainder term in Eq. (2) is represented by the simple potential in Eq. (13) for the DFT–fragment interaction. For the fragment–fragment interaction this potential has the form of a simple, exponential function

$$V_m^{\mathrm{rep}}(\mu,s)=\sum_j^J c_{m,j}(\mu)e^{-\alpha_{m,j}(\mu)r_{m,s}}, \quad (18)$$

where $J=4$, the atomic centers and the center of mass. The coefficients and exponents for the two repulsion potentials were optimized in separate calculations. For the fragment–fragment potential the set of 192 water dimer geometries,

TABLE V. DFT–fragment screening parameters.

	Coefficient	α (exponent)
O1	0.186 119	0.549 105
H2	0.112 182	0.389 541
H3	0.112 182	0.389 541
BO21	−0.717 580	0.962 143
BO31	−0.717 580	0.962 143

TABLE VI. Components of the localized molecular polarizabilities. The expansion points are at the centroids of the localized molecular orbitals.

	XX	*YY*	*ZZ*	*XY*	*XZ*	*YX*	*YZ*	*ZX*	*ZY*
LMO1	0.003 10	0.004 55	0.002 82	0.000 00	0.000 00	0.000 00	0.000 00	0.000 00	0.0000
LMO2	2.1093	0.835 17	1.5561	0.000 00	1.3139	0.000 00	0.000 00	0.934 52	0.0000
LMO3	2.1093	0.835 17	1.5561	0.000 00	−1.3139	0.000 00	0.000 00	−0.934 52	0.0000
LMO4	1.5195	0.736 18	1.1830	0.000 00	0.000 00	0.780 91	0.000 00	0.000 00	0.0890
LMO5	1.5195	0.736 18	1.1830	0.000 00	0.000 00	−0.780 91	0.000 00	0.000 00	−0.0890

shown schematically in Fig. 1, was used to model the potential energy surface of the H_2O dimer. The figure shows all orientations that were used for the water dimer. For each orientation shown in the figure, several O–O distances were included. The best result, in terms of both the rms value for the fit itself and good agreement with the DFT water dimer structure and interaction energy, was accomplished for the set in which the weighting factor [w_p in Eq. (14)] is set to unity, as it was in EFP1/HF, and the cutoff value for the water–water interaction energy is set to 15 kcal/mol. All structures with an energy more repulsive than the cutoff were removed from the fitting set. This value is high enough on the repulsion wall that all relevant dimer structures are still taken into account: there are 177 surface points below the cutoff. The rms deviation for this set is very good: 0.56 kcal/mol.

For the fitting of the DFT–fragment interaction, a subset of 28 structures was used. These 28 structures represent the equilibrium hydrogen bonded water dimer structure, as represented in Fig. 2, with 14 different O–O distances. The DFT density was frozen and the fragment molecule was moved around it generating the set of 28 structures. For the DFT–fragment interaction, the fragment H-donor and H-acceptor may exhibit different behavior due to different charge–transfer interactions. Therefore, for each orientation both fragment H-donor and H-acceptor were included. The rms

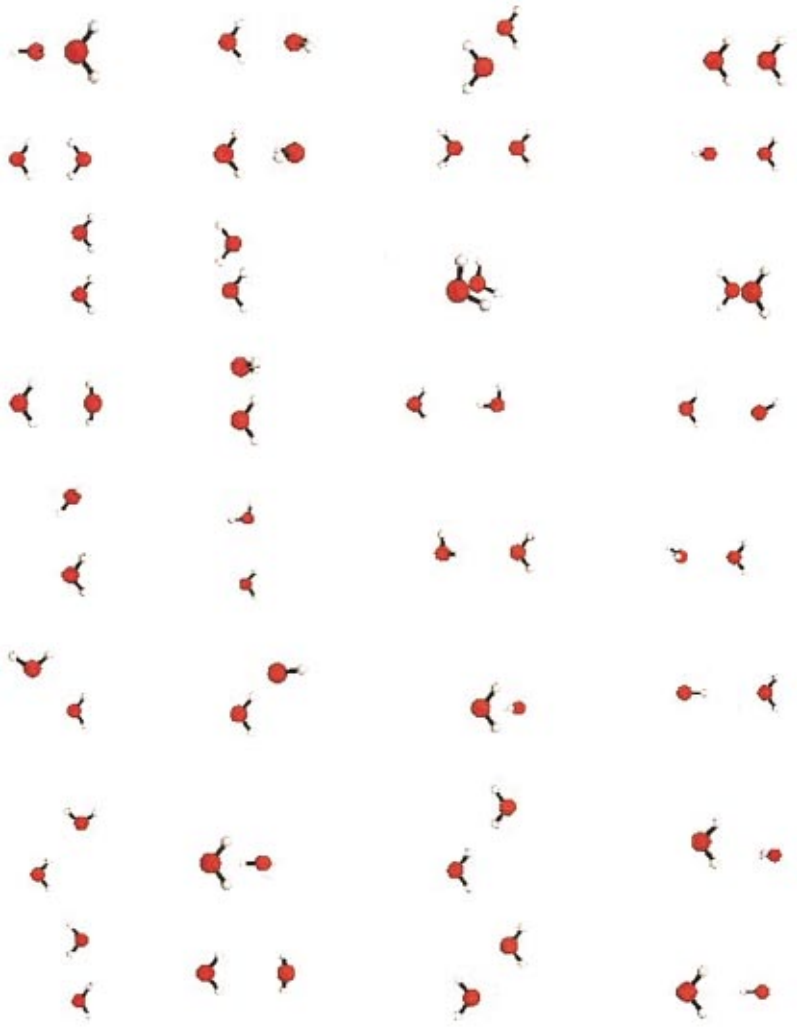

FIG. 1. (Color) A schematic of the 192 water dimer orientations.

FIG. 2. (Color) Equilibrium water dimer orientation.

for fitting the coefficients and exponents in the DFT–fragment case is 2.1 kcal/mol. This value is greater than desired, due to the wide range of energies that are included in the fitting set: in order to treat both very attractive and repulsive structures, energies included in the fit range from +18.00 to −0.75 kcal/mol. It is difficult to fit very repulsive structures using a small number of parameters, but they are needed to balance attractive forces in the model. This set, despite a somewhat greater rms than desired, manages to do this reasonably well.

IV. TEST CALCULATIONS

Now that all of the DFT based parameters for both the fragment–fragment and DFT–fragment interaction energies have been determined and the gradient has been derived the new method can be carefully tested for its ability to treat water clusters as well as chemical reactions in water. In this section several test applications are presented.

A. Water dimer

Water dimer, as the smallest of all water clusters, has been studied extensively.[22,23] So, this is a useful system to test the DFT based EFP method. The effective fragment potential must be tested for both mixed dimers: H donor DFT/H acceptor EFP and vice versa, since the two water molecules in the water dimer are not equivalent. Using the DH (*d, p*) basis set, a full DFT optimization was performed on the water dimer. The binding energy and structural parameters are compared among all DFT, all EFP and mixed DFT–EFP calculations. The results are presented in Table VII. The difference in the structure between the two mixed DFT–EFP cases is due to an unsymmetrical charge transfer energy contribution, which is difficult to simulate in a parametrized approach. It is also important to note that the EFP1/DFT potential energy surface is very flat, so that different structures can have similar energies. The greatest deviation from the DFT binding energy is 0.7 kcal/mol, for the EFP/EFP case, and the greatest deviation from the DFT hydrogen bond distance is 0.08 A. For the mixed EFP–DFT dimers, the predicted interaction energies bracket the all-DFT value, with errors of 0.4 and 0.6 kcal/mol. In all cases shown in Table VII, the correct water dimer orientation is reproduced.

TABLE VII. Interaction energy for water dimer (kcal/mol) and H–O distance (Å).

	Binding energy	H–O distance
All DFT	6.67	1.901
H acceptor–DFT	7.08	1.885
H acceptor–fragment	6.48	1.822
All EFP	7.37	1.822

TABLE VIII. Harmonic frequencies (cm^{-1}) of water dimer for DFT–DFT, DFT–EFP, EFP–DFT, and EFP–EFP case. Percent deviations from all DFT are given in parentheses.

DFT	H acceptor =DFT	H acceptor =EFP	EFP
128.91	129.55 (1%)	140.09 (9%)	147.03 (15%)
159.87	150.39 (6%)	222.46 (38%)	221.30 (38%)
167.76	152.08 (9%)	201.65 (20%)	224.95 (33%)
204.86	251.48 (22%)	262.73 (28%)	311.38 (51%)
410.55	356.41 (13%)	494.68 (20%)	439.31 (7%)
682.94	626.78 (8%)	740.85 (8%)	727.17 (6%)
RMS=0	33	55	59

A vibrational analysis was carried out for four different representations of water dimer: all DFT, DFT–EFP, EFP–DFT, and EFP–EFP. The results of the harmonic vibrational analysis are summarized in Table VIII. The overall trend of the values for the frequencies is reproduced for both mixed DFT–EFP and EFP–EFP. The quantitative agreement with the all DFT case ranges from 1 to 60 cm^{-1} depending on the vibrational mode. The rms deviations from the DFT result are also given in Table VIII, with the relative deviations with respect to the all DFT case given in parentheses.

B. Water clusters

Small water clusters have been the subject of many theoretical[24–26] studies. The most commonly studied properties of the clusters are their structures and binding energies. One of the main goals in the development of the EFP1/DFT method was improvement in the treatment of the water clusters, especially their binding energies. The original, EFP1/HF method, performs very well in terms of prediction of the *relative* energies for small[5(a)] and large water clusters,[5(b)] but since it is based on HF theory, EFP1/HF cannot reproduce experimental binding energies, because correlation effects play an important role in determining these binding energies.

EFP1/DFT calculations on small water clusters were performed as a test of the fragment–fragment interaction energy. Table IX lists the binding energies for the lowest energy isomers for the water trimer, tetramer, and hexamer. The absolute agreement between EFP1/DFT and DFT calculations is very good, ranging from 0.9 to 1.3 kcal/mol. Also listed in Table IX are the binding energies per water molecule. The DFT and EFP1/DFT values are in good qualitative agreement. In particular, the EFP method captures the increase in the binding energy per molecule with the increase of the size of the cluster.

The next test of the model is the prediction of the relative and binding energies for the five lowest energy isomers of the water hexamer.[5(b)] These structures were optimized using both B3LYP and EFP1/DFT, with the DH (*d, p*) basis set, and their binding energies were calculated. Results are compared with previously reported MP2 and CCSD(T) calculations[5(b)] in Table X. For internal consistency all calculations were performed with the DH (*d, p*) basis set. Experimental evidence[5(b)] suggests that the cage structure is the global minimum on the potential energy surface of the water

TABLE IX. Water trimer, tetramer, and hexamer binding energies (kcal/mol). The binding energy per molecule is given in parentheses.

	DFT binding energy	All fragments binding energy
Trimer	21.56 (7.19)	20.23 (6.74)
Tetramer	37.72 (9.43)	36.85 (9.21)
Hexamer	62.37 (10.39)	61.08 (10.13)

hexamer. B3LYP, MP2, CCSD(T), and EFP1/HF all predict the same isomer order, with the prism structure found to be more stable than the cage by approximately 0.5 kcal/mol, and cyclic and boat predicted to be the two highest isomers. EFP1/DFT inverts the order of the first three isomers, but the energy spread is only about 0.7 kcal/mol. This is within the expected accuracy of the EFP1/DFT method. With regard to binding energies, the incorporation of electron correlation effects in both B3LYP and EFP1/DFT methods is apparent, given their much better agreement with the MP2 binding energies, than with HF. It is important to note, however, that all of the binding energies listed in Table X are too large due to the basis set deficiencies. Xantheas and co-workers[26(b)] have calculated these binding energies for MP2 at the complete basis set limit. They find binding energies on the order of 44–46 kcal/mol for the water hexamer isomers.

C. Glycine–3H_2O system

The glycine system has been treated previously using both combined supermolecular-continuum[27–29] and continuum approaches.[30] The system was also studied with the EFP1/HF method.[9,29] It has been noted that both electrostatic and correlation effects are important in determining the neutral–zwitterion equilibrium.[29] In this study, test calculations were performed on the lowest energy neutral (*N*) and zwitterion (*Z*) structure of glycine in the presence of three water molecules. The glycine structures used in this study correspond to the one reported by Kassab *et al.*[31] and Bandyopadhyay and Gordon.[29] The whole system was treated with DFT, using the B3LYP functional and the 6-31++G (d,p) basis set. Geometry optimization was done for the *trans* isomer of the neutral glycine (TN) form, using both DFT/B3LYP and EFP1/DFT method, because it has been shown[29] that this is the lowest energy structure on the potential energy surface. Figure 3 shows these optimized structures. For the zwitterion (*Z*) isomer the lowest energy structure is the *cis* isomer. The relative energies of these two isomers calculated with DFT and EFP1/DFT are given in Table XI.

TABLE X. Binding energies (kcal/mol) for the five lowest isomers of the water hexamer.

	B3LYP	EFP1/DFT	MP2	CCSD(T)	HF	EFP1/HF
Prism	62.37	61.08	58.25	55.10	42.86	42.42
Cage	61.84	61.53	57.52	54.30	42.49	41.90
Book	61.34	61.79	56.49	53.10	42.44	41.45
Cyclic	60.57	60.65	55.75	52.20	43.10	41.14
Boat	59.13	59.37	54.29	50.80	42.12	40.09

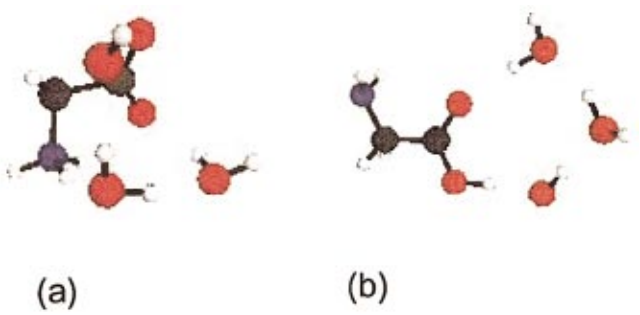

FIG. 3. (Color) Optimized structures of (a) *cis*-zwitterion cluster (Z) and (b) *trans*-neutral (TN) cluster with three water molecules using B3LYP/6-31++G (*d, p*), with EFP1/DFT waters.

These results are compared with the previous MP2, HF, and EFP1/HF results. First, consider the EFP1/HF, HF, and MP2 results. The first two of these are in excellent agreement, and both predict that TN is about 15 kcal/mol higher in energy than Z. As noted above, correlation plays a key role in this relative energy, since MP2 decreases this energy difference by about 10 kcal/mol, with TN still more stable by about 4 kcal/mol. Since DFT includes correlation effects, the DFT/B3LYP level of theory also stabilizes Z relative to TN, although by only 7 kcal/mol. At this level of theory TN is lower than Z by about 8 kcal/mol. This effect is captured by the EFP1/DFT method, which predicts TN to be about 6 kcal/mol lower than Z.

This is an important result, since it illustrates the essential purpose for the development of the EFP1/DFT method—the incorporation of correlation effects into the EFP methodology. The results in Table XI also illustrate[29] that three water molecules are not sufficient enough to stabilize the zwitterion that it is the global minimum.

V. CONCLUSIONS

The methodology of the effective fragment potential (EFP) method has been adopted and implemented at the density functional level of theory, using the hybrid B3LYP functional. The DFT based EFP represents a first step in the direction of a complete treatment of the correlation effects inside the EFP solvation method. Preliminary tests for different aspects of the method are encouraging. The overall agreement with full DFT results is on the order of $\leqslant$2 kcal/mol. The DFT based EFP results are also closer to more accurate, higher order *ab initio* calculations. Future work, will involve inclusion of generalized charge transfer and dis-

TABLE XI. Relative HF/6-31++G(d,p), MP2/6-31++G(d,p), B3LYP/6-31++G(d,p), and EFP1/DFT energies of the *cis*-Z glycine $(H_2O)_3$ and *trans*-N glycine$(H_2O)_3$ (in kcal/mol).

	Relative energy TN–ZC
DFT	8.00
EFP1/DFT	5.83
HF	15.6
EFP1/HF	14.7
MP2	4.3

persion contributions into the model, and continuation of the development of the transferable, general EFP2[13–16] approach, for the treatment of different solvents.

ACKNOWLEDGMENTS

The authors would like to thank Professor Jan H. Jensen, Dr. Walter J. Stevens, and Dr. Paul N. Day for many helpful discussions. This work was supported by a grant from the Air Force Office of Scientific Research.

[1] (a) L. Onsager, J. Am. Chem. Soc. **58**, 1486 (1936); (b) C. J. Cramer and D. G. Thrular, in *Reviews in Computational Chemistry*, edited by D. B. Boyd and K. B. Lipkowitz (VCH, New York, 1995), Vol. 6; (c) C. J. Cramer and D. G. Thrular, in *Solvent Effects and Chemical Reactivity*, edited by O. Tapia and J. Bertran (Kluwer Academic, Dordrecht, the Netherlands, 1996); (d) J. Tomasi and M. Perisco, Chem. Rev. **94**, 2027 (1994).
[2] (a) A. Warshel, J. Phys. Chem. **83**, 1640 (1979); (b) R. M. Levy, D. B. Kitchen, J. T. Blair, and K. J. Krogh-Jespersen, *ibid.* **94**, 4470 (1990); (c) B. T. Thole and P. T. van Duijnen, Theor. Chim. Acta **55**, 307 (1980).
[3] Feature article by P. N. Day, J. H. Jensen, M. S. Gordon, S. P. Webb, W. J. Stevens, M. Krauss, D. Garmer, H. Basch, and D. J. Cohen, Chem. Phys. **105**, 1968 (1996).
[4] (a) W. Chen and M. S. Gordon, J. Chem. Phys. **105**, 11081 (1996); (b) S. P. Webb and M. S. Gordon, J. Phys. Chem. A **103**, 1265 (1999).
[5] (a) G. N. Merrill and M. S. Gordon, J. Phys. Chem. A **102**, 2650 (1998); (b) P. N. Day, R. Pachter, M. S. Gordon, and G. N. Merrill, J. Chem. Phys. **112**, 2063 (2000).
[6] (a) M. Krauss, Comput. Chem. (Oxford) **19**, 199 (1995); (b) M. Krauss and B. D. Wladowski, Int. J. Quantum Chem. **69**, 11 (1998); (c) M. Krauss and S. P. Webb, J. Chem. Phys. **107**, 5771 (1997).
[7] H. Li, A. W. Hains, J. E. Everts, A. D. Robertson, and J. H. Jensen, J. Phys. Chem. B **106**, 3486 (2002).
[8] R. M. Minikis, V. Kairys, and J. H. Jensen, J. Phys. Chem. A **105**, 3829 (2001).
[9] (a) P. Bandyopadhyay and M. S. Gordon, J. Chem. Phys. **113**, 1104 (2000). (b) P. Bandyopadhyay, M. S. Gordon, B. Mennucci, and J. Tomasi, J. Phys. Chem. **116**, 12 (2002).
[10] (a) R. G. Parr and W. Yang, in *International Series of Monographs on Chemistry 16*, edited by R. Breslow, J. B. Goodenough, J. Halpern, and J. S. Rowlinson (Oxford University Press, New York; Clarendon, Oxford, 1989); (b) W. Koch and M. C. Holthausen, *A Chemist's Guide to Density Functional Theory* (Wiley–VCH, Verlag, GmbH, 2000).
[11] (a) A. D. Becke, Phys. Rev. A **38**, 3098 (1988); (b) C. Lee, W. Yang and R. G. Parr, Phys. Rev. B **37**, 785 (1988).
[12] For the specific flavor of the B3LYP used, consult GAMESS manual: http://www.msg.ameslab.gov/GAMESS/doc.menu.html
[13] M. S. Gordon, A. M. Freitag, P. Bandyopadhyay, J. H. Jensen, V. Kairys, and W. J. Stevens, J. Phys. Chem. A **105**, 293 (2001).
[14] J. H. Jensen, J. Chem. Phys. **104**, 7795 (1996).
[15] J. H. Jensen and M. S. Gordon, Mol. Phys. **89**, 1313 (1996).
[16] J. H. Jensen and M. S. Gordon, J. Chem. Phys. **108**, 4772 (1998).
[17] (a) A. J. Stone, Chem. Phys. Lett. **83**, 233 (1981); (b) A. J. Stone, *The Theory of Intermolecular Forces* (Oxford University Press, Oxford, 1996).
[18] M. A. Freitag, M. S. Gordon, J. H. Jensen, and W. J. Stevens, J. Chem. Phys. **112**, 7300 (2000).
[19] T. H. Dunning, Jr. and P. J. Hay, in *Methods of Electronic Structure Theory*, edited by H. F. Shaefer (Plenum, New York, 1977), Chap. 1, pp. 1–27.
[20] M. W. Schmidt, K. K. Baldridge, J. A. Boatz, *et al.*, J. Comput. Chem. **14**, 1347 (1993).
[21] S. F. Boys, in *Quantum Science of Atoms, Molecules, and Solids*, edited by P. O. Lowdin (Academic, New York, 1966), pp. 253–262.
[22] S. Simon, M. Duran, and J. J. Dannenberg, J. Phys. Chem. A **103**, 1640 (1999).
[23] A. D. Estrin, L. Paglieri, G. Corongiu, and E. Clementi, J. Phys. Chem. **100**, 8701 (1996).
[24] S. Maheshwary, N. Patel, N. Sathyamurthy, A. D. Kulkarin, and R. Gadre, J. Phys. Chem. A **105**, 10525 (2001).
[25] H. M. Lee, S. B. Suh, J. Y. Lee, P. Tarakeshwar, and S. K. Kim, J. Chem. Phys. **112**, 9759 (2000).
[26] (a) B. L. Grigorenko, A. V. Nemukhin, I. A. Topol, and S. K. Brut, J. Chem. Phys. **113**, 2638 (2000); (b) S. S. Xantheas, C. J. Burnham, and R. J. Harrison, *ibid.* **116**, 1493 (2002).
[27] H. S. Rzepa and M. Y. Yi, J. Chem. Soc., Perkin Trans. 1 **24**, 531 (1991).
[28] J. H. Jensen and M. A. Gordon, J. Am. Chem. Soc. **117**, 8159 (1995).
[29] P. Bandyopadhyay, M. S. Gordon, B. Mennucci, and J. Tomasi, J. Chem. Phys. **116**, 5023 (2002).
[30] See references from Ref. 29: (a) R. Bonaccorsi, P. Palla, and J. Tomasi, J. Am. Chem. Soc. **106**, 1945 (1984); (b) T. N. Truong and E. V. Stefanovich, J. Chem. Phys. **103**, 3709 (1995); (c) J. Andzelm, C. Kolmel, and A. Klamt, *ibid.* **103**, 9312 (1995); (d) L. Gontrani, B. Mennucci, and J. Tomasi, J. Mol. Struct.: THEOCHEM **500**, 113 (2000).
[31] E. Kassab, J. Langlet, E. Evleth, and Y. Akacem, J. Mol. Struct.: THEOCHEM **531**, 267 (2000).